

Achieving effective artifact subspace reconstruction in EEG using real-time video-based artifact identification

Sunghyun Kang
School of Electrical Engineering
and Computer Science
Gwangju Institute of Science
and Technology (GIST)
Gwangju, Republic of Korea
kanghyun51015@gm.gist.ac.kr

Kyungho Won
School of Electrical Engineering
and Computer Science
Gwangju Institute of Science
and Technology (GIST)
Gwangju, Republic of Korea
kyunghowon0712@gm.gist.ac.kr

Heegy Kim
School of Electrical Engineering
and Computer Science
Gwangju Institute of Science
and Technology (GIST)
Gwangju, Republic of Korea
kim0401hg@gist.ac.kr

Jihoon Baek
School of Electrical Engineering
and Computer Science
Gwangju Institute of Science
and Technology (GIST)
Gwangju, Republic of Korea
jihoon0536@gm.gist.ac.kr

†

Minkyu Ahn
School of Computer Science
and Electrical Engineering
Handong Global University
Pohang, Republic of Korea
minkyuahn@handong.edu

Sung Chan Jun*
School of Electrical Engineering
and Computer Science /
AI Graduate School
Gwangju Institute of Science
and Technology (GIST)
Gwangju, Republic of Korea
scjun@gist.ac.kr

Abstract—Identifying and minimizing physiological artifacts in EEG is challenging because these artifacts may corrupt the underlying brain activity severely. In this work, we proposed a hybrid approach to detect/reduce EEG artifacts by combining the MediaPipe face mesh model and artifact subspace reconstruction (ASR). Four types of artifacts, eye blinking, horizontal/vertical eye movements, and jaw movement during EEG measurement were generated to test our approach. We observed that real-time video-based artifact identification achieved over 95% accuracy in detecting eye blinking, horizontal eye movement, and jaw movement. Moreover, the targeted noise reduction was effective in analyzing the signal-to-noise ratio (SNR) for each specific artifact. This work may contribute to improving the reliability and accuracy of EEG data analysis in the real-world and online scenarios by providing a practical and effective approach to identifying and reducing physiological artifacts in real-time.

Keywords—electroencephalography (EEG), artifacts, image processing, artifact detection

I. INTRODUCTION

Electroencephalography (EEG) is used widely to measure brain signals in various fields because of its non-invasive, simple application, and good temporal resolution [1]. However, EEG studies, including brain-computer interfaces (BCI) and mobile brain-body imaging (MoBI), have encountered challenges in achieving high signal-to-noise ratio

(SNR) because of such physiological artifacts as electrooculography (EOG), electromyography (EMG), or motion artifacts that may interfere with other useful information, such as event-related potentials (ERP) [2-4].

To target and reduce these physiological artifacts, many studies have proposed various EEG methods or other hybrid approaches, such as independent component analysis (ICA), and principal component analysis (PCA), etc. [5-8]. Most research has focused not only on targeting the motion artifacts, but also removing or reducing them. Further, the demand for automated methods to classify and reduce noise in real-time in BCI is inevitable because practical BCI systems require real-time analysis and its implementation [9]. One of the popular real-time physiological artifact reduction schemes is artifact subspace reconstruction (ASR) which is used commonly in BCI. However, it cannot remove the noise sources selectively, which may lead to the loss of necessary information [10-11]. Nonetheless, in general, a customizable scheme to identify and reduce physiological artifacts from targeted noise sources in real-time is quite rare in the BCI field [12].

In some cases, a multimodal approach using image information in EEG has been applied to identify emotion or vigilance that is related strongly to facial recognition [13-14]. In addition, an open-source fast motion detection model that requires relatively less calculation, such as MediaPipe, has been introduced in a recent study and has strong potential to be implemented in practical scenarios without special hardware requirements, such as an eye tracker [15]. This approach is promising, as it enhances EEG's temporal

This work was supported by the IITP (Institute of Information and Communications Technology Planning & Evaluation) grants (No. 2017-0-00451, No. 2019-0-01842) funded by the Korea government.

resolution, and thus it has the potential to be implemented in EEG as a multimodal appliance. However, similar implementation to inspect physiological movements that affect the EEG signal is relatively rare in current studies.

Given such limitations, we proposed a multimodal approach in EEG to identify and reduce only targeted artifacts. In this work, we considered four types of physiological artifacts—eye blinking, horizontal/vertical eye movement, and jaw movement. To this end, an artifact detection methodology based upon MediaPipe and targeted ASR based upon the detection information, were implemented. The feasibility of our approach was verified by inspecting the EEG signals' grand mean in the time domain and the signal-to-noise ratio (SNR) difference between the original resting EEG and targeted ASR-implemented EEG.

II. METHODS

A. Artifacts Detection Methods

The MediaPipe face mesh model was introduced in a real-time artifact detection scheme to detect artifacts rapidly [15]. This model produces 468 3D facial landmarks with normalized coordinates based upon information in the image of the human face. In this work, we used facial information to detect eye blinking, horizontal eye movement, vertical eye movement, and jaw movement. The right/left sides denote the right/left side of the person who is tracked in the video. Thus, four physiological artifacts were defined and their corresponding detection algorithms are described as follows:

- Eye blinking task: To detect eye blinking, eye aspect ratio (EAR) was introduced with the following equation [16]:

$$EAR = \frac{\sqrt{(L_{2x}-L_{6x})^2+(L_{2y}-L_{6y})^2} + \sqrt{(L_{3x}-L_{5x})^2+(L_{3y}-L_{5y})^2}}{\sqrt{(L_{1x}-L_{4x})^2+(L_{1y}-L_{4y})^2}}, \quad (1)$$

in which L_{px} and L_{py} refer to the x and y coordinates of selected p landmarks, as illustrated in Fig 1. For eyes open to eyes closed, the detection threshold was set as when the EAR value decreased to less than 0.22, while eyes closed to open was set as when the EAR value increased to higher than 0.3 [16]. EAR was estimated for the left and right eyes separately. Finally, eye blinking was defined when one of those eyes' EAR value was reported as the eyes closed.

- Horizontal/vertical eye movement task: The virtual origin was introduced in eyeball range according to the following equation (2). The MediaPipe face mesh model provides the real-time iris location (right eye iris landmark I_R : 472, left eye iris landmark I_L : 477); thus, this information was used to locate the iris in the coordinate as well as to calculate the Euclidian distance from the virtual origin (equation (3)).

$$O = \left(\frac{L_{4x}+L_{3x}+L_{7x}+L_{8x}}{4}, \frac{L_{4y}+L_{3y}+L_{7y}+L_{8y}}{4} \right), \quad (2)$$

$$D = \sqrt{(I_x - O_x)^2 + (I_y - O_y)^2}, \quad (3)$$

in which I_x and I_y refer to the x and y of the iris landmarks selected. The movement of left/right eyes

was tracked separately, and the beginning of the movement was defined as when the difference in the distance D from the previous video frame to the current frame was more than 0.0005, while the end of the movement was defined as when the difference in the distance was less than 0.0005.

- Jaw movement: To detect jaw movement, we used the facial landmarks from the nose (landmark L_n : 1), mouth (upper lip landmark L_u : 13, lower lip landmark L_l : 14), and chin (landmark L_c : 199) locations, and the following ratio was used [17]:

$$D_{nc} = \sqrt{(L_{nx} - L_{cx})^2 + (L_{ny} - L_{cy})^2}, \quad (4)$$

$$D_m = \sqrt{(L_{ux} - L_{lx})^2 + (L_{uy} - L_{ly})^2}, \quad (5)$$

$$\text{Ratio} = \frac{D_m}{D_{nc}}. \quad (6)$$

The detection of jaw open to closed was defined as when the ratio was less than 0.05, while jaw closed to open was defined as when the ratio was higher than 0.05.

The predicted labels were sent as event markers to the EEG streams. In this study, we integrated the MediaPipe into OpenViBE, which is an open-source software for BCI and real-time processing of brain signal [18]. Using socket communication, we tagged the predicted labels into the EEG streams played in OpenViBE scenario, as illustrated in Fig. 2. As a result, the predicted labels could be synchronized with the EEG data. For the precise information regarding TCP tag format, refer to the [OpenViBE documentation page](#).

B. Apparatus

In this study, a workstation with Intel i7-6700 CPU (with NVIDIA RTX 2070 Super graphics card) was used to detect real-time physiological artifacts, acquire EEG, and present the stimulus. Note that the artifact detection model ran as delegated with CPU.

EEG was recorded from 32 scalp EEG channels based upon the international 10-20 system with an extra 4 channels, the left/right mastoids and left horizontal & top-left vertical EOG channels (ActiveTwo, BioSemi Inc. Netherland) at a

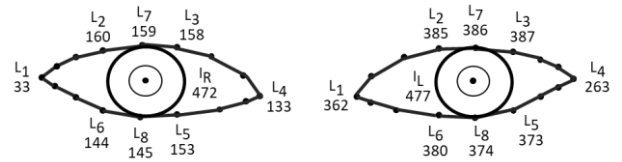


Fig. 1. MediaPipe face mesh landmark location in left/right eyes.

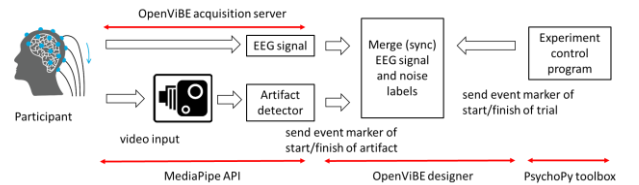


Fig. 2. Proposed framework for identifying and reducing physiological artifacts.

512 Hz sampling rate. To identify image-based artifacts, a front webcam (c920HD, Logitech Inc.) mounted at the center of the screen was used to stream 30 fps video with 1,080p resolution; the input video to the MediaPipe face mesh was rescaled to 480p for efficiency.

The PsychoPy toolbox aided the control program during the experiment [19]. OpenViBE created an event marker when the cue was given/finished in the control program or the internal TCP/IP connection received the artifact information detected. This relation is illustrated in detail in Fig. 2.

C. Procedure of Experiment

Five healthy adults (age 28.6 ± 3.66 yrs., four males) were recruited for the preliminary experiment approved by the Gwangju Institute of Science and Technology (GIST) Institutional Review Board (20230504-HR-71-03-02). First, the participants were asked to fill out questionnaires about their current states, related diseases that may affect performing the tasks, and the adult attention-deficit hyperactivity disorder (ADHD) self-report scale-v.1.1. (ASRS-v1.1) to check the feasibility of the experiment [20]. The participants sat in a comfortable chair and maintained a distance of 60 cm between the center of the screen and their eyes. Then, the resting state EEG was recorded. After the recording, the participants were asked to undergo 30 trials for each movement task in random order. These procedures are described in Fig. 3.

- Rest state: Participants were asked to open their eyes when the cross appeared and to rest when the cross disappeared. The cross was displayed for 5 seconds and disappeared for 5 seconds. Eyes-open EEG was recorded for 4 minutes 30 seconds during the rest state.
- Eye blinking: Participants were instructed to blink one time only when the cross disappeared. The cross was displayed for 2 seconds and disappeared for 1 second.
- Horizontal eye movement: Participants were instructed to move their eyes and follow the cross without moving their head/body. Eye blinking was prohibited during this task. The cue was given as the cross moved in a horizontal direction (left-to-right, right-to-left). This action took 1 second, and the moving cross was stopped for 0.5 seconds before it continued to move.
- Vertical eye movement: this followed the same procedure as horizontal eye movement, but the participants followed the cross as it moved up-to-down or down-to-up.

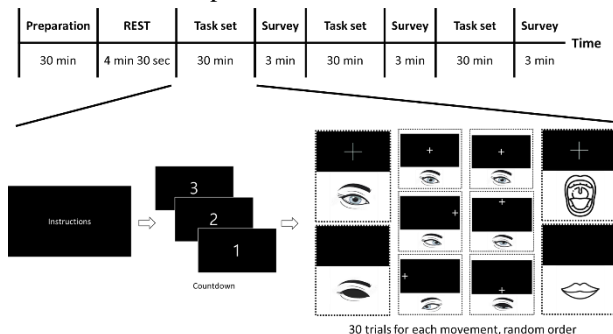


Fig. 3. Experimental procedure diagram.

- Jaw movement: The participants were instructed to open their jaw and mouth as widely as possible when the cross appeared and close the jaw and mouth when it disappeared. The cross was displayed for 2 seconds and disappeared for 1 second.

After one task session (four tasks, 120 trials per session), the participants were asked to fill out the questionnaires to self-evaluate their fatigue and capability to continue the next task using 5-point Likert scales (1: not tired at all, 5: too tired). The questionnaires were filled out right after each task session. All participants performed three sessions; thus, a total of 360 trials (90 per movement) were collected for each participant.

D. Artifact Detection Analysis

To evaluate the artifact detection methods' temporal resolution, the actual frame rate at which the detection framework ran was collected during the experiment. Further, bad trials were removed when the participant failed to perform the specific movement tasks for a given cue. In addition, we note that 30 trials of the eye blinking task (20 trials for subject 1, 10 trials for subject 2) were removed because of unrecorded video. The accuracy with which artifacts was detected was evaluated according to whether the artifact information was observed successfully when the cue was given to the subject. This was accomplished by inspecting the synchronized video and EEG signals manually.

E. EEG Preprocessing

As shown in Table I, additional bad trials were removed when the participant performed multiple movements in a particular task (e.g., performed eye blinking with jaw movement during the jaw movement task); otherwise, abnormal EEG signals would be detected. The number of bad trials for subject 1 during jaw movement was relatively higher than those of the other participants. This may be attributable to xerophthalmia (i.e., dry-eye syndrome), which the participant reported in the survey.

MATLAB-based EEGLAB and FieldTrip toolboxes were used primarily to preprocess and analyze the EEG data [21-22]. EEG data were first band-pass filtered with cutoff frequencies of 0.5 and 50 Hz using the 4th order Butterworth filter. Then filtered data were re-referenced to the Cz electrode channel to minimize the artifacts caused by facial muscles, as applied in the previous study [5]. Thereafter, we extracted epochs as follows: one seconds after the onset (eye blinking and eye movements) and two seconds after the onset (jaw movement).

TABLE I. NUMBER OF TRIALS COLLECTED

Subject	Physiological artifacts (Image/EEG trials)			
	Eye blinking	Horiz. eye movement	Vert. eye movement	Jaw movement
1	68/68	85/85	89/89	90/5
2	79/79	89/89	90/90	90/78
3	87/87	88/86	87/85	90/80
4	90/89	89/85	89/86	90/74
5	86/86	86/84	81/81	90/73

F. Noise Reduction

In this work, noise reduction was managed by artifact subspace reconstruction (ASR), which repeatedly computing principle component analysis (PCA) on EEG data covariance to detect artifacts [10]. EEG covariance from the eye-open rest state was computed; and ASR was applied based upon each movement's start marker (rising edge) to finish marker (falling edge). To inspect ASR in the real-time noise reduction scenarios, the range to apply ASR in the time domain was set in three ways: between 100 ms before the rising edge and 100 ms after the falling edge, between 400 ms before the rising edge and 400 ms after the falling edge, and in the time domain overall.

For the targeted noise reduction observations, the grand mean in both the time and frequency domains was inspected. To demonstrate whether the noise from the movement artifacts was removed successfully, the grand mean was calculated for each movement from the trials (# of trials for each artifact is listed in Table I). Thus, it shows the grand mean of the trials overall for all 31 channels of the scalp EEG. Further, the signal's log power spectrum in the frequency domain was compared.

The artifact signal-to-noise ratio (SNR) was used measuring the performance in reducing the targeted noise [23]. EEG signals were transformed by fast Fourier transform (FFT) and separated into five spectral bands: delta (0.5 – 4 Hz), theta (4 – 8 Hz), alpha (8 – 12 Hz), beta (12 – 30 Hz), and gamma (30 – 50 Hz). Then, artifact SNR values were estimated for each band as follows:

$$P_{\text{artifact}} = \frac{1}{N_{\text{artifact bins}}} \sum_{i=w_1}^{w_h} x_i^2, \quad (7)$$

$$P_{\text{average}} = \frac{1}{N_{\text{all bins}}} \sum_{i=w_1}^{w_h} x_i^2, \quad (8)$$

$$\text{SNR}_{\text{artifact}} = 10 \log_{10} \left(\frac{P_{\text{artifact}}}{P_{\text{average}}} \right). \quad (9)$$

Here, x_i refers to the signal in the band range selected, $w_1 \sim w_h$ refer to the selected frequency bands, N_{bins} refers to the number of signal elements in a selected band range, P_{artifact} refers to the power between the rising and falling edge of the artifact detected in one cue, and P_{average} refers to the power overall in the same cue. Thus, $\text{SNR}_{\text{artifact}}$ refers to the artifact power to signal power ratio, and the noise attributable to physiological artifacts is defined as the power difference between $\text{SNR}_{\text{artifact}}$ and the SNR in the rest state overall [5].

To observe whether the targeted physiological artifacts were reduced successfully, SNR analysis was conducted by estimating the absolute SNR difference between the band-passed (0.5 – 50 Hz) EEG signals for each band in a noisy state with specific noise reduction (100 ms or 400 ms) and ASR was applied to the EEG signals for the subjects overall.

III. RESULTS AND DISCUSSION

A. Temporal Resolution and Accuracy of Artifact Detection

From the artifact detection framework, frames per second of the video input were collected. Then the reciprocal value of the frame rate was calculated as tabulated in Table II. These results showed that the mean temporal resolution of the artifact detection framework was approximately 48 ~ 49 ms

and the standard error was less than 0.25 ms. This verified that the artifact detection temporal resolution was good at approximately 50 ms.

The accuracy with which each artifact was detected (for artifact trials in Table I) is tabulated in Table III. The accuracy in detecting eye blinking was 95.85%, which is similar to that in previous studies of EAR [16]. However, subject 5 in particular demonstrated poor performance in detecting eye blinking as well as horizontal/vertical eye movement.

B. Noise Reduction in Time Domain

To identify the targeted noise reduction mechanism, visual inspection of the grand mean in the time domain was performed for each subject, as described in Fig. 4, in which ASR (100 ms) refers to the real-time scenario ASR that was applied 100 ms before the rising edge/after the falling edge, ASR (400 ms) represents noise reduction when the ASR range was changed to 400 ms before the rising edge/after the falling edge, and ASR (all) refers to ASR applied in the time domain overall. Note that in the jaw movement task, the falling edge did not appear because participants opened their mouth when the jaw open cue appeared after 2 seconds of the jaw close cue.

Here, it is noticeable that the noise attributable to each artifact was reduced between the rising and the falling edges. However, the artifacts remained after the reduction when the ASR range was not sufficiently good in the eye-blinking and jaw movement tasks compared to ASR (400 ms) or ASR applied in the range overall. Thus, in a real-time scenario (ASR (100 ms)) with our proposed artifact detection framework, it may be possible that some noise artifacts remained even though ASR was applied. Further, from the brain power spectrum perspective, physiological artifacts are observed in the bands overall, particularly in the temporal region, and those artifacts were removed when the ASR with

TABLE II. TEMPORAL RESOLUTION OF ARTIFACT DETECTION

Subject	Temporal resolution (mean ± standard error, milliseconds)			
	Eye blinking	Horiz. eye movement	Vert. eye movement	Jaw movement
1	48.65 ± 0.21	48.64 ± 0.21	48.84 ± 0.22	48.50 ± 0.19
2	48.77 ± 0.21	48.83 ± 0.22	48.77 ± 0.21	48.70 ± 0.20
3	49.03 ± 0.22	48.93 ± 0.22	49.14 ± 0.23	48.84 ± 0.20
4	48.73 ± 0.21	48.86 ± 0.22	48.79 ± 0.21	48.65 ± 0.20
5	48.81 ± 0.22	48.89 ± 0.22	48.87 ± 0.21	48.81 ± 0.20

TABLE III. ARTIFACT DETECTION ACCURACY

Subject	Detection accuracy			
	Eye blinking	Horiz. eye movement	Vert. eye movement	Jaw movement
1	100 %	97.65 %	96.63 %	100 %
2	100 %	100 %	82.22 %	100 %
3	100 %	97.73 %	78.82 %	92.22 %
4	100 %	100 %	85.39 %	100 %
5	80.23 %	88.37 %	49.38 %	100 %
Total	95.85 %	96.80 %	78.67 %	98.44 %

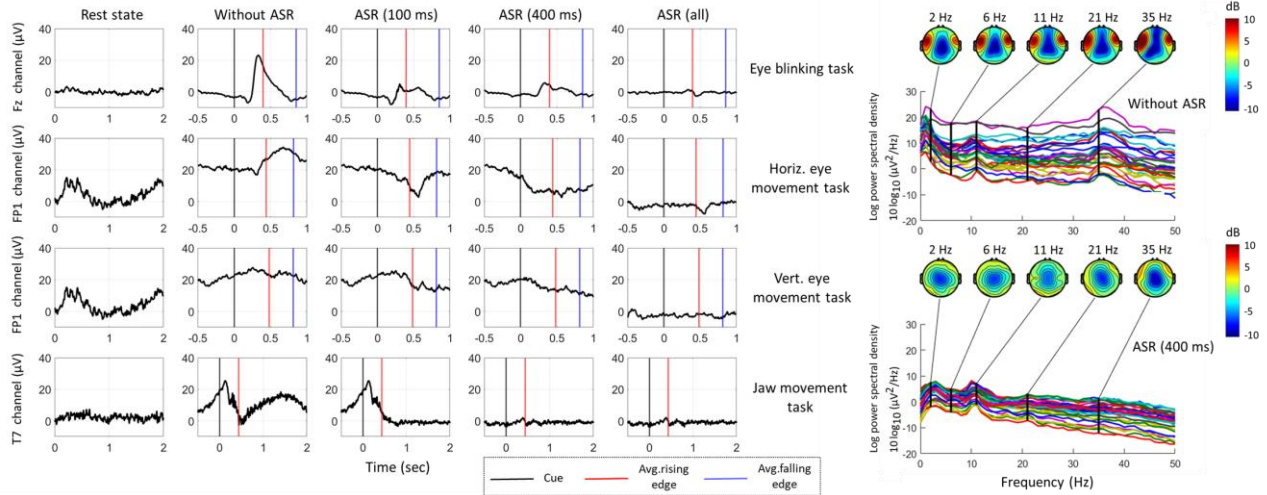


Fig. 4. Physiological artifacts and artifact-free segments. The left figure represents the trial-averaged waveforms for each physiological artifacts and artifact-free segments depending on ASR time resolutions for subject 5. The black, red, and blue vertical lines indicate the cue and rising/falling edge of noise detection, respectively. The right figure represents logarithm of power spectral density before/after ASR for jaw movement for subject 4.

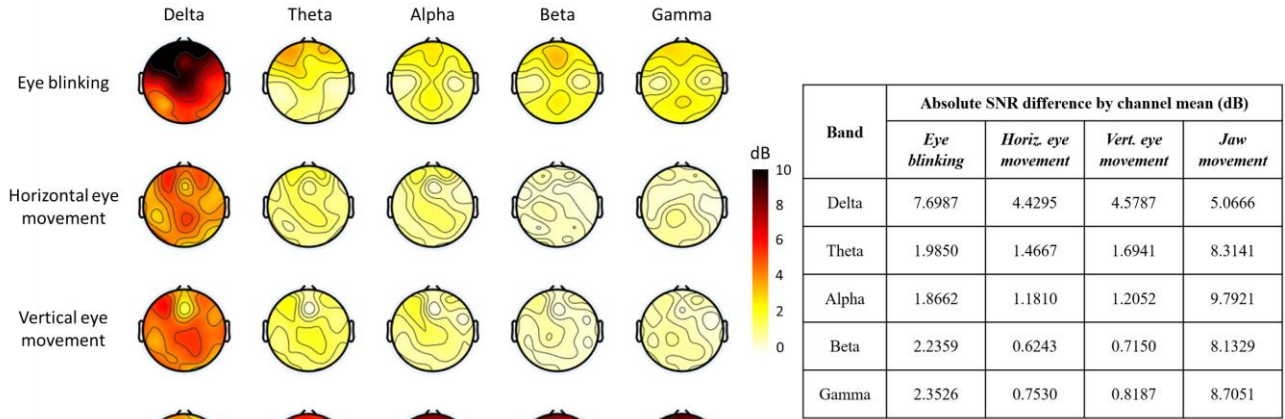


Fig. 5. Absolute SNR difference between artifact and artifact-free data. Left scalp topography plots represent SNR difference between artifact and artifact-free data over the brain, and the right table tabulates absolute values for SNR difference values for each movement tasks/bands by averaging channels overall (except for the reference channel – Cz).

a moderate time range (400 ms) was applied. Thus, to achieve targeted noise reduction, it appears that a modest range for ASR is approximately 400 ms.

C. SNR Analysis

To analyze the SNR, an average SNR difference plot is shown in Fig. 5 for each band range. Here, it is observed that in the eye blinking task, the SNR difference over the frontal channels was relatively higher in the delta and theta bands. Further, the eye blinking task showed a relatively higher SNR difference in the delta band compared to other bands. Hence, it may be inferred that the distinctive eye blinking artifacts were removed effectively [2]. This tendency is similar to the horizontal/vertical eye movements in the SNR difference of the delta band; however, the SNR difference was less compared to that in the eye blinking task, which has been reported in a previous study [5]. In addition, both tasks showed relatively small SNR differences in the alpha, beta, and gamma bands compared to the delta band. Jaw movement showed a relatively higher SNR difference in the theta, alpha, beta, and gamma band ranges compared to the delta band

region. Further, it showed a relatively greater SNR difference in the temporal region compared to other regions. Hence, it appears that our proposed targeted ASR detected and reduced jaw movement artifacts effectively [3].

D. Limitations and Future Directions

As shown in Table II, although the temporal resolution of real-time facial movement detection appeared to be stable at approximately 50 ms, the actual temporal resolution or total latency from detecting an artifact to EEG labeling was not evaluated in this work. Although the internal TCP/IP connection is known to have quite a brief latency, assessment of the precise latency should be conducted in future work because this may not reduce noise completely in the real-time application, as shown in Fig. 4 [24]. The accuracy with which artifacts were detected in subject 5 was poor, which may be attributable to different light conditions compared to the other 4 participants. This sensitivity to the light environment has been reported in another study [25], so it may be critical to control the light environment strictly. In addition, detection of vertical eye movement was relatively less accurate compared

to other movements, and hence, adjusting the movement threshold or introducing other detection methods should be considered in future research. Further, this framework did not use trained model-based artifact detection because it compromises the framework's temporal resolution, although it may permit artifacts to be detected more accurately.

Although ASR is known to be suitable for real-time noise reduction and its implementation in real-time has been assessed, this work did not actually apply ASR in a real-time scenario. Further, there is some possibility that noise will not be reduced completely (Fig. 4). Thus, it may be necessary to adjust ASR implementation somewhat for the user's purpose. In addition, this work did not perform a comparison with other real-time noise reduction methods, which is under investigation currently.

Finally, the assessment of this framework under the complex physiological artifacts (e.g., head movement during eye blinking) for generalized manner was not explored here, which is our utmost goal and is underway.

IV. CONCLUSION

This work showed the possibility of combining multimodal data with EEG, not only to identify artifacts, but also to reduce noise. To enable this, a real-time facial artifact tracking model with detection algorithms was combined with streaming EEG signals. The results showed that the temporal resolution of detecting artifacts was approximately 50 ms; the accuracy in detecting eye blinking, horizontal eye movement, and jaw movement was more than 95%, while vertical eye movement was approximately 80% accurate. The grand mean and SNR difference analysis showed that each artifact was reduced objectively in EEG signals based upon the rising edge/falling edge from the artifact detection framework. Hence, this work contributes to improving the reliability of EEG data analysis by providing a practical approach to identify physiological artifacts in real-time and reduce them in a targeted manner.

REFERENCES

- [1] J. Wolpaw, N. Birbaumer, D. McFarland, G. Pfurtscheller, and T. Vaughan, "Brain-computer interfaces for communication and control", *Clinical Neurophysiology*, vol. 113, no. 6, pp. 767-791, 2002.
- [2] R. N. Roy, S. Charbonnier, and S. Bonnet, "Eye blink characterization from frontal EEG electrodes using source separation and pattern recognition algorithms", *Biomedical Signal Processing and Control*, vol. 14, pp. 256-264, 2014.
- [3] I. I. Goncharova, D. J. McFarland, T. M. Vaughan, and J. R. Wolpaw, "EMG contamination of EEG: spectral and topographical characteristics", *Clinical neurophysiology*, vol. 114, no. 9, pp. 1580-1593, 2003.
- [4] Y. P. Lin, Y. Wang, and T. P. Jung, "A mobile SSVEP-based brain-computer interface for freely moving humans: The robustness of canonical correlation analysis to motion artifacts", *2013 35th Annual International Conference of the IEEE Engineering in Medicine and Biology Society (EMBC)*, Osaka, Japan, 2013, pp. 1350-1353.
- [5] S. L. Kappel, D. Looney, D. P. Mandic, and P. Kidmose, "Physiological artifacts in scalp EEG and ear-EEG", *Biomedical engineering online*, vol. 16, no. 1, pp 1-16, 2017.
- [6] M. K. Islam, A. Rastegarnia, and Z. Yang, "Methods for artifact detection and removal from scalp EEG: A review", *Neurophysiologie Clinique/Clinical Neurophysiology*, vol. 46, no. 4-5, pp. 287-305, 2016.
- [7] M. M. N. Mannan, M. A. Kamran, and M. Y. Jeong, "Identification and Removal of Physiological Artifacts From Electroencephalogram Signals: A Review", *IEEE Access*, vol. 6, pp. 30630-30652, 2018.
- [8] D. Gorjan, K. Gramann, K. De Pauw, and U. Marusic, "Removal of movement-induced EEG artifacts: current state of the art and guidelines", *Journal of neural engineering*, vol. 19, no. 1, 2022.
- [9] J. Minguillon, M. A. Lopez-Gordo, and F. Pelayo, "Trends in EEG-BCI for daily-life: Requirements for artifact removal", *Biomedical Signal Processing and Control*, vol. 31, pp. 407-418, 2017.
- [10] T. R. Mullen, C. A. Kothe, Y. M. Chi, A. Ojeda, T. Kerth, S. Makeig, T.P. Jung, and G. Cauwenberghs, "Real-time neuroimaging and cognitive monitoring using wearable dry EEG", *IEEE Transactions on Biomedical Engineering*, vol. 62, no. 11, pp. 2553-2567, 2015.
- [11] C. Y. Chang, S. H. Hsu, L. Pion-Tonachini, and T. P. Jung, "Evaluation of Artifact Subspace Reconstruction for Automatic Artifact Components Removal in Multi-Channel EEG Recordings", *IEEE Transactions on Biomedical Engineering*, vol. 67, no. 4, pp. 1114-1121, 2020.
- [12] C. R. Rashmi and C. P. Shantala, "EEG artifacts detection and removal techniques for brain computer interface applications: a systematic review", *International Journal of Advanced Technology and Engineering Exploration*, vol. 9, no. 88, pp. 354-383, 2022.
- [13] Y. Huang, J. Yang, P. Liao, and J. Pan, "Fusion of facial expressions and EEG for multimodal emotion recognition", *Computational intelligence and neuroscience*, vol. 2017, 2017.
- [14] W. L. Zheng and B. L. Lu, "A multimodal approach to estimating vigilance using EEG and forehead EOG", *Journal of neural engineering*, vol. 14, no. 2, 2017.
- [15] C. Lugaresi, J. Tang, H. Nash, C. McClanahan, E. Uboweja, M. Hays, F. Zhang, C. L. Chang, M. Yong, J. Lee, W.T. Chang, W. Hua, M. Georg, and M. Grundmann, "Mediapipe: A framework for perceiving and processing reality", *Third Workshop on Computer Vision for AR/VR at IEEE Computer Vision and Pattern Recognition (CVPR)*, Long Beach, CA, USA, 2019, vol. 2019.
- [16] T. Soukupova and J. Cech, "Eye blink detection using facial landmarks", *21st computer vision winter workshop*, Rimske Toplice, Slovenia, 2016, p. 2.
- [17] R. Chinthala, S. Katkoori, C. S. Rodriguez, and M. J. Mifsud, "An Internet of Medical Things (IoMT) Approach for Remote Assessment of Head and Neck Cancer Patients", *2022 IEEE International Symposium on Smart Electronic Systems (iSES)*, Warangal, India, 2022, pp. 124-129.
- [18] Y. Renard, F. Lotte, G. Gibert, M. Congedo, E. Maby, V. Delannoy, O. Bertrand, and A. Lécuyer, "Openvibe: An open-source software platform to design, test, and use brain-computer interfaces in real and virtual environments", *Presence*, vol. 19, no. 1, pp. 35-53, 2010.
- [19] J. Peirce, J. R. Gray, S. Simpson, M. MacAskill, R. Höchenberger, H. Sogo, E. Kastman, and J. K. Lindeløv, "PsychoPy2: Experiments in behavior made easy", *Behavior research methods*, vol. 51, pp. 195-203, 2019.
- [20] J. H. Kim, E. H. Lee, and Y. S. Joung, "The WHO Adult ADHD Self-Report Scale: reliability and validity of the Korean version", *Psychiatry investigation*, vol. 10, no. 1, pp. 41-46, 2013.
- [21] A. Delorme and S. Makeig, "EEGLAB: an open source toolbox for analysis of single-trial EEG dynamics including independent component analysis", *Journal of Neuroscience Methods*, vol. 134, no. 1, pp. 9-21, 2004.
- [22] R. Oostenveld, P. Fries, E. Maris, and J. M. Schoffelen, "FieldTrip: Open source software for advanced analysis of MEG, EEG, and invasive electrophysiological data," *Computational Intelligence and Neuroscience*, vol. 2011, pp. 1-9, 2011.
- [23] B. Somers, T. Francart, and A. Bertrand, "A generic EEG artifact removal algorithm based on multi-channel Wiener filter", *Journal of neural engineering*, vol. 15, no. 3, 2018.
- [24] T. V. Lakshman and U. Madhow, "The performance of TCP/IP for networks with high bandwidth-delay products and random loss", *IEEE/ACM Transactions on Networking*, vol. 5, no. 3, pp. 336-350, 1997.
- [25] X. Zhou, "Eye-Blink Detection under Low-Light Conditions Based on Zero-DCE", *2022 IEEE Conference on Telecommunications, Optics and Computer Science (TOCS)*, Dalian, China, 2022, pp. 1414-1417.